

## Sn-isotope fractionation as a record of hydrothermal redox reactions

JUNMING YAO<sup>1</sup>, RYAN MATHUR<sup>2,\*</sup>, WAYNE POWELL<sup>3</sup>, BERND LEHMANN<sup>4</sup>, FERNANDO TORNOS<sup>5</sup>,  
MARC WILSON<sup>6</sup>, AND JOAQUIN RUIZ<sup>7</sup>

<sup>1</sup>Key Laboratory of Mineralogy and Metallogeny, Guangzhou Institute of Geochemistry, Chinese Academy of Sciences, Guangzhou, China

<sup>2</sup>Department of Geology, Juniata College, Huntingdon, Pennsylvania 16652, U.S.A.

<sup>3</sup>Department of Earth and Environmental Sciences, Brooklyn College, City University of New York, Brooklyn 11210, New York, U.S.A.

<sup>4</sup>Mineral Resources, Technical University of Clausthal, Clausthal-Zellerfeld, Germany

<sup>5</sup>Instituto de Geociencias (CSIC-UCM), Madrid, Spain

<sup>6</sup>Carnegie Museum of Natural History, Pittsburgh, Pennsylvania 15213, U.S.A.

<sup>7</sup>University of Arizona, Tucson, Arizona 85712, U.S.A.

### ABSTRACT

A redox reaction in which Sn<sup>2+</sup> oxidizes to Sn<sup>4+</sup> is thought to occur during the precipitation of cassiterite (SnO<sub>2</sub>) and stannite (Cu<sub>2</sub>FeSnS<sub>4</sub>) from high-temperature hydrothermal solutions. In four stanniferous regions with differing mineralization environments (South Dakota, U.S.A.; Cornwall, England; Erzgebirge, Germany/Czech Republic; Andean tin belt, Bolivia), the tin isotope composition in stannite (mean value  $\delta^{124}\text{Sn} = -1.47 \pm 0.54\%$ ,  $n = 21$ ) is consistently more fractionated toward negative values than that of paragenetically earlier cassiterite (mean value  $\delta^{124}\text{Sn} = 0.48 \pm 0.62\%$ ,  $n = 50$ ). Given the oxidation-dependent mechanism for cassiterite precipitation, this isotopic shift is most likely attributable to the oxidation of Sn in solution; precipitation of heavy-Sn-enriched cassiterite results in residual dissolved Sn with lighter isotopic composition, which is expressed in the negative  $\delta^{124}\text{Sn}$  values of later-formed stannite. Equally important is that the mean values for the cassiterite from the various deposits are slightly different and may indicate that the initial Sn isotope composition in early-formed cassiterite relates to variations in the source or magmatic processes. Therefore, the Sn isotopes may provide information on both redox reactions and petrologic sources and processes.

**Keywords:** Tin isotopes, cassiterite, stannite, metal isotope fractionation, redox

### INTRODUCTION

Tin has been an economically significant metal since it was first alloyed with copper to produce bronze nearly 7000 yr ago (Radivojevic et al. 2013). Tin exhibits complex behavior, acting as a volatile, siderophile, and chalcophile element, and may exist in the Sn<sup>0</sup>, Sn<sup>2+</sup>, or Sn<sup>4+</sup> valence state. Although it is rare, with an average crustal abundance of 1.7 ppm (Rudnick and Gao 2003), it has the largest number of naturally formed isotopes (10) and exhibits the greatest mass range (112–124 amu) of any element on the periodic table. Given that the degree of isotopic fractionation is related, in part, to the relative mass difference of the isotopes, the large mass range of Sn may allow for the monitoring of fractionation of a heavy metal that is typically associated with hydrothermal systems related to felsic magmatism (Lehmann 1990).

Measurable isotopic fractionation of tin has been reported for ores (Haustein et al. 2010), igneous rocks (Creech et al. 2017; Badullovich et al. 2017), and archaeological bronze artifacts (Balliana et al. 2013; Yamazaki et al. 2014; Mason et al. 2016). The isotopic variation measured in these materials indicates that high-temperature geological processes fractionate tin isotopes. Only Badullovich et al. (2017) has presented evidence for an associated mechanism that induces an isotopic variation of tin, i.e.,

partitioning of Sn<sup>4+</sup> between magma and ilmenite during fractional crystallization of basalt. However, no studies have focused on the processes and materials associated with tin mineralization: highly evolved felsic magmas, involvement of a saline hydrothermal fluid, rapidly evolving redox conditions, and distinct mineral assemblages in which cassiterite (SnO<sub>2</sub>) is predominant. Without an understanding of causative mechanisms of fractionation in typical hydrothermal tin ore systems, interpretation of Sn isotopic data by geologists and archaeologists is limited.

Tin experiences electron transfer in high-temperature geochemical reactions, including those associated with the precipitation of cassiterite in tin mineralizing systems (Eugster and Wilson 1985). The precipitation of cassiterite is likely dominated by the reactions associated with the oxidation of Sn-chloride complexes, such as:

$$\text{Sn}^{2+}\text{Cl}_x^{2-x} + 2\text{H}_2\text{O} = \text{Sn}^{4+}\text{O}_2 + 2\text{H}^+ + x\text{Cl}^- + \text{H}_2 \text{ (Heinrich 1990)}$$
and

$$\text{SnCl}_3 + \text{H}^+ + 2\text{H}_2\text{O} = \text{SnO}_2 + 3\text{HCl} + \text{H}_2 \text{ (Korges et al. 2018)}.$$

Based on fluid inclusion analysis and mineral stability studies, cassiterite precipitation from hydrothermal solutions can occur across a wide temperature range (320–550 °C), although the main phase of cassiterite precipitation in most ores typically occurs within the temperature range of approximately 400–350 °C (Campbell and Panter 1990; Markl and Schumacher 1996;

\* E-mail: mathurr@juniata.edu

Korges et al. 2018).

Redox reactions are known to fractionate isotopes in numerous metal systems (e.g., Cu and Fe). Furthermore, inelastic nuclear resonant X-ray scattering (INRXS) and Mössbauer spectroscopy experiments predict that oxidation state has a large effect on fractionation of Sn (from  $\delta^{122}\text{Sn} = 0.4$  to 4.1‰ for  $\text{Sn}^{2+}$  and  $\text{Sn}^{4+}$  species) within the range of temperatures associated with tin mineralization (300–700 °C) (Polyakov et al. 2005). Thus, fractionation associated with oxidation may account for much of the observed isotopic variation in this metal. Accordingly, the purpose of this study is to empirically evaluate and model the role of redox reactions as a mechanism for Sn isotope fractionation in association with hydrothermal processes by comparing Sn isotope values for paragenetically early and late tin minerals. The early formation of cassiterite and the late formation of stannite in hydrothermal systems is well established from detailed ore microscopy work on classical tin provinces (Cornwall: Jackson et al. 1982; Bolivia: Kelly and Turneure 1970; Spain: Chicharro et al. 2016).

#### RATIONALE FOR REDOX REACTIONS AS A MECHANISM FOR SN ISOTOPE FRACTIONATION

In well-studied multi-valent transition metal isotopic systems such as Cu and Fe, it has been established that redox reactions impart significant fractionation, with oxidation favoring the heavier isotope in low-temperature reactions (Zhu 2002; Borrok et al. 2008; Pokrovsky et al. 2008; Mathur et al. 2010). Given that Sn undergoes a redox reaction in hydrothermal fluids during mineralization, it is likely that the electron transfer required for the formation of cassiterite or soluble  $\text{Sn}^{4+}$ -complexes will favor the heavier isotopes of tin.

The solubility of tin in granitic magmas is redox dependent. Experimental studies have demonstrated that under reducing conditions, where tin exists predominantly in the  $\text{Sn}^{2+}$  state, cassiterite solubility is orders of magnitude greater than under oxidizing conditions where  $\text{Sn}^{4+}$  is the dominant stable species (Linnen et al. 1995, 1996). Oxygen fugacity values for tin granites lie between the QFM and NNO buffer, allowing for high dissolved  $\text{Sn}^{2+}$  contents (Heinrich 1990) that become further concentrated in differentiated water- and halogen-rich residual magmas (Lehmann 1982). In addition, Linnen et al. (1996) concluded that peraluminous granites have a greater  $\text{Sn}^{2+}/\text{Sn}^{4+}$  ratio than that of other granite compositions. Subsequent work demonstrated that the dominance of  $\text{Sn}^{2+}$  in peraluminous granites persists over a wide range of redox conditions (QFM to QFM+2.4) (Farges et al. 2006).

Due to the redox and compositional dependence of Sn solubility in granitic magmas, primary Sn-mineralization is associated with ilmenite-series granites, typically peraluminous that derive their low- $f_{\text{O}_2}$  character from the partial melting of organic-bearing sedimentary rocks (Lehmann 1982; Černý et al. 2005). At shallow crustal levels, tin will partition to exsolved aqueous hydrothermal fluids, predominantly as  $\text{Sn}^{2+}$ -chloride complexes (Eugster 1985).

Cassiterite ( $\text{SnO}_2$ ) is the primary economic tin mineral, and its precipitation from reduced, magma-derived hydrothermal fluids requires electron transfer to produce  $\text{Sn}^{4+}$ . Possible triggers for oxidation of hydrothermal fluids include mixing with meteoric

waters, pH change due to progressive hydrolysis (greisen development), or vapor separation (e.g., Heinrich 1990). Oxidation of tin within peraluminous magma may also result in cassiterite nucleation because  $\text{Sn}^{4+}$  cannot be accommodated in the melt structure (Farges et al. 2006). Regardless of the specific process and site associated with mineralization, redox reactions are essential to the genesis of all primary cassiterite ores.

#### TIN IN MINERALS, GRANITES, AND ORES

Recent direct U-Pb dating of hydrothermal cassiterite and U-Pb zircon ages of associated granite have confirmed the coeval timing of hydrothermal mineralization with late-stage granite magmatism (Yuan et al. 2011; Chen et al. 2014; Zhang et al. 2015, 2017). Ore is spatially associated with apical positions of cupolas that are composed of the latest-stage differentiates of larger bodies of tin granite, and in which Sn-enriched volatiles accumulate (e.g., Groves 1972; Plimer 1987). If the magma is emplaced at sufficiently shallow depths, ultimately, hydrothermal brines are released by hydraulic fracturing of the granitic carapace (Plimer 1987).

Ores associated with tin granites commonly exhibit a mineralogical zoning pattern where tin, in the form of cassiterite, is concentrated proximal to the granite contact, whereas Cu-Pb-Zn sulfide ores form at greater distance or overprint earlier cassiterite in proximal parts of the system. Tin in sulfides is usually in low abundance, most commonly in the form of stannite ( $\text{Cu}_2\text{FeSnS}_4$ ), and forms later in the paragenetic sequence compared to cassiterite (Sillitoe et al. 1975; Sugaki et al. 1981; Lehmann 1987; Chicharro et al. 2016). Tin is present in the  $\text{Sn}^{4+}$  state in both cassiterite and stannite, with the cation valences in stannite being  $\text{Cu}_2^+\text{Fe}^{2+}\text{Sn}^{4+}\text{S}_4$  (Eibschütz et al. 1967; Greenwood and Whitfield 1968).

Early cassiterite precipitation results from oxidation, either associated with hydrolysis of feldspars (greisenization) or mixing with meteoric waters (Heinrich 1990; Heinrich and Ryan 1992; Chicharro et al. 2016). Late-stage Sn-sulfide assemblages precipitate due to pressure and temperature decrease associated with higher-level hydraulic fracturing, further mixing with meteoric water, and further oxidation due to the liberation of  $\text{H}_2$  vapor (Heinrich and Ryan 1992; Chicharro et al. 2016). This mixing provides an additional source of reduced sulfur, cools and dilutes the hydrothermal brine, but does not introduce additional Sn (Heinrich and Ryan 1992). Thus, each hydrothermal tin mineralizing system is associated with a single localized Sn source (highly differentiated granite) and a single magmatic-hydrothermal fluid (Korges et al. 2018); this fluid undergoes progressive oxidation during its ascent. If oxidation favors the heavier isotopes of Sn, then cassiterite precipitation would leave the remaining  $\text{Sn}^{2+}$  in solution enriched in the lighter isotopes. Within an ore deposit, this isotopic shift would be expected to be recorded in the contrasting Sn isotope composition of the paragenetically earlier cassiterite (heavy isotope enriched) and late-stage stannite (light isotope enriched).

Isolating the contribution of redox reactions to Sn fractionation may be impeded by overprints associated with additional fractionation mechanisms.  $\text{Sn}^{4+}$  may substitute for Ti in various oxides and silicates, potentially resulting in isotopic partitioning between coexisting mineral phases. In tin granites, biotite may contain as much as 1000 ppm Sn (Neiva 1976; Imeokparia 1982; Wang et al. 2013). Titanite ( $\text{CaTiSiO}_5$ ) and malayaite ( $\text{CaSnSiO}_5$ ) form a solid

solution. Near end-member malayaite has been documented in Sn-skarns from New South Wales (Plimer 1984), and titanite with as much as 26 wt% SnO<sub>2</sub> has been reported from granites in southern China (Xie et al. 2010; Wang et al. 2013). Other Sn-bearing minerals in skarns and granites include garnet, clinopyroxene, magnetite, and rutile (Plimer 1984; Wang et al. 2013). Given the complexity of Sn-bearing mineral assemblages in both granites and skarns, this study emphasizes the mineralogically simpler ores associated with veins and greisens within silicate host rocks.

Tin deposits display considerable variation but can be classified based on their relative depth, position relative to the granite contact, and style of mineralization (Taylor 1979). Herein, we examine classic localities from four distinct styles of tin mineralization (Fig. 1).

(1) Deposits associated with batholithic magmatic environments (e.g., Erzgebirge) in which extensive quartz-muscovite-topaz replacement (greisenization) with disseminated cassiterite is predominant over large-scale veining, and the majority of mineralization lies within, or immediately above, granite cupolas. At Cinovec (Zinnwald) in the Erzgebirge, cassiterite ore is hosted predominantly by greisens formed under lithostatic pressures, with lesser ore within approximately coeval veins that developed under hydrostatic conditions at a depth of 2–3 km and at temperatures between 335 and 410 °C (Korges et al. 2018).

(2) Deposits associated with granitoids of deep subvolcanic character (e.g., Cornwall) in which brittle fracturing is more common than greisenization, and most mineralization occurs above granite cupolas. Veins commonly exhibit greisenized selvages. Most Cornish tin occurs in steeply dipping lode veins

with exploitable strike lengths of hundreds to thousands of meters. The main tin lodes consist of quartz-tourmaline-cassiterite, and are barren of sulfides (Jackson et al. 1989). Homogenization temperatures for these veins range from 275 to 400 °C (Jackson et al. 1982; Smith et al. 1996). Stanniferous sulfide-bearing chloritic lodes are less abundant and contain cassiterite-chlorite assemblages with subsequent precipitation of pyrite-chalcopyrite-stannite-sphalerite (Bromley and Holl 1986) at 200–380 °C (Jackson et al. 1982). Mineralization was emplaced at depths of 2–5 km (Smith et al. 1996).

(3) Deposits associated with subvolcanic settings (e.g., Bolivia, Cenozoic porphyry samples) and deep subvolcanic character (e.g., northern Bolivia, Triassic tin granites), which are dominated by brittle fracture systems above the apical zone of small intrusions. Cassiterite is the most abundant ore mineral of tin and occurs primarily in quartz, quartz-tourmaline, or quartz-sulfide veins that formed between 510 and 250 °C (Sugiyaki and Kitakaze 1988). Stannite-chalcopyrite-sphalerite-bearing veins postdate main-stage cassiterite mineralization, at 350–230 °C (Sillitoe et al. 1975; Sugaki and Kitakaze 1988). Depths of emplacement are estimated to be between 350 and 2000 m (Kelly and Turneure 1970), which implies that the hydrothermal fluids consisted of both liquid and vapor.

(4) Pegmatite-hosted disseminated ores of magmatic origin (e.g., Black Hills, South Dakota, U.S.A.). Sub-ore-grade cassiterite mineralization occurs in the Li-pegmatites of the Keystone region of South Dakota, including the Etta deposit where cassiterite is intergrown with spodumene and feldspar, as well as disseminated within a muscovite-albite matrix (Schwartz 1925). Stannite also occurs in the Li-pegmatites of the Etta deposit where it is intergrown with chalcopyrite, chalcocite, and bornite (Connolly 1916). At the nearby Peerless pegmatite, stannite occurs as nodules at the margin of the quartz cores of pegmatite bodies (Černý et al. 2001). The timing relationship between cassiterite and stannite at these localities is uncertain, the importance of these types of deposits is that the ores formed in a deep setting at ≥8 km depth, as documented by the spodumene-quartz assemblage (London 1984).

## METHODOLOGY

Four examples of tin mineralization were selected spanning the four mineralization styles described above, each hosting both cassiterite and stannite: South Dakota, U.S.A. (pegmatite), Cornwall, U.K. (vein-dominated); Cinovec-Krupka camp of the Erzgebirge, Czech Republic (greisen-dominated); Potosi, Bolivia (porphyry). The approach compares minerals from different Sn mineralization styles as a means to identify similar physiochemical reactions across the broad spectrum of tin deposits. The selection of both early cassiterite and late stannite from contrasting settings allows for the evaluation of redox reactions as a potential fractionating mechanism across a range of mineralizing environments.

Due to the fact that the ores are from historic mining districts, all samples are derived from museum collections, and each reported isotope value is from one distinct mineral sample. Samples were obtained from the American Museum of Natural History in New York and the Carnegie Museum of Natural History in Pittsburgh.

Different methods were employed to extract Sn from cassiterite and stannite. Several techniques have been suggested for reduction of Sn from cassiterite (Hausteint et al. 2010; Yamazaki et al. 2014; Brüggmann et al. 2017) due to its resistance to acid dissolution. In this contribution, the methodology of Mathur et al. (2017), a refinement of Hausteint et al. (2010), was used: 0.25 g of –100 mesh cassiterite powder was mixed with 1 g of KCN and heated at 850 °C for 1 h in graphite crucibles. The resulting reduced Sn metal beads were dissolved in heated ultrapure 11 N HCl overnight. For stannite, 0.05 g of powdered sample was dissolved in 15 mL polytetrafluoroethylene jars with ultrapure aqua regia plus trace HF that was

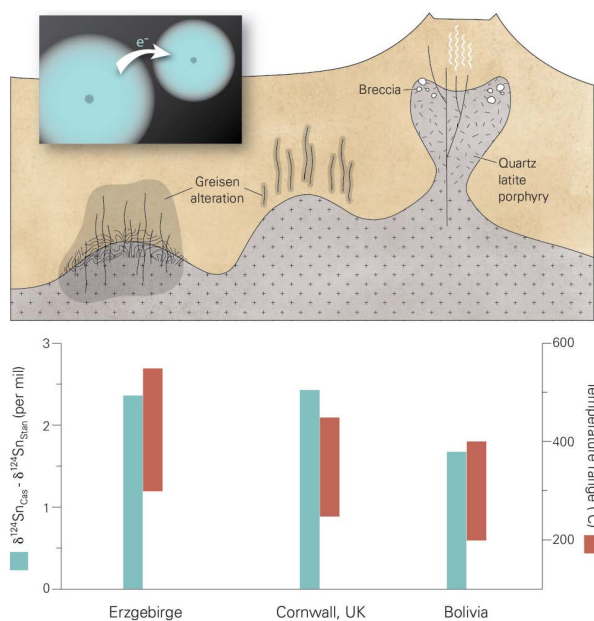


**FIGURE 1.** Cartoon cross section depicting key differences in the deposit types analyzed along with Sn isotope difference between cassiterite and stannite for deposits analyzed. Oxidation reactions at high temperatures induce distinct isotopic signatures. The example from South Dakota would be a significantly greater depth with pegmatitic fluids being the source of mineralization. (Color online.)

heated (100 °C) for 12 h. Complete dissolution was confirmed visually.

For both cassiterite and stannite, a small aliquot was removed and dried for ion exchange chromatography. Solutions were purified using ion exchange chromatography described in Balliana et al. (2013), and employed by Mason et al. (2016) and Mathur et al. (2017). Volumetric yield calculations confirmed the dissolution and recovery of greater than 95% of all Sn from the reduced Sn metal of cassiterite and dissolved stannite samples.

Samples were measured on the Isoprobe at the University of Arizona. Aqueous sample introduction into the plasma was achieved by free aspiration using a microconcentric borosilicate glass nebulizer. Sample uptake rate was approximately 100–150 µL/min. Solutions were kept at 150 ppb, which generated a 3–4 V signal intensity for <sup>120</sup>Sn. The cups were arranged with <sup>119</sup>Sn on the axial mass. The remaining mass positions were as follows; <sup>116</sup>Sn on low 3, <sup>117</sup>Sn on low 2, <sup>120</sup>Sn on H1, <sup>121</sup>Sb on H2, <sup>122</sup>Sn on H3, <sup>123</sup>Sb on H4, and <sup>124</sup>Sn on H5. The instrument interface was fitted with Ni sample and skimmer cones. The argon gas flow rate of the hexapole collision cell on the Isoprobe was set at 2.5 mL/min. Rinse times between samples was approximately 2–3 min. Background intensity for <sup>120</sup>Sn ranged from 0.8–1 mV. On-peak blank subtraction was applied to each measurement. Sample measurement consisted of one block of thirty 10 s integration measurements. The intensity of the unknowns matched the signal intensity of the bracketing standard within 20%. Measuring the standard between a 2–5 V signal on <sup>120</sup>Sn did not produce errors larger than reported.

Mass bias was corrected for by using Sb-doped solutions (High-Purity ICP-MS Sb standard 10 2–3; 10 µg/mL in 2% nitric and trace HF) and an exponential mass bias correction defined in Mathur et al. (2017). The corrected values were then bracketed with the NIST 3161A Sn standard. One block of 25 ratios was collected and all samples were measured in duplicate. Data are presented relative to the NIST 3161A Sn standard (Lot no. 07033) in per mil notation defined as:

$$\delta^{1xx}\text{Sn}\text{‰} = \left( \frac{\left( \frac{1xx_{\text{Sn}}}{116_{\text{Sn}}} \right)_{\text{sample}}}{\left( \frac{1xx_{\text{Sn}}}{116_{\text{Sn}}} \right)_{\text{NIST 3161}}} - 1 \right) \cdot 1000.$$

Whole procedural 1σ errors for analysis are δ<sup>120</sup>Sn = 0.04‰ and δ<sup>124</sup>Sn = 0.08‰ (0.01‰ per amu) for cassiterite as reported in Mathur et al. (2017). This error was calculated by measuring the same sample over 20 times in an effort to refine the reduction procedure and define full procedural errors. Stannite was dissolved and did not experience the KCN reductions. Therefore, the error for stannite measurements is most likely lower. However, the error reported for cassiterite is assumed to be a conservative estimate of errors on stannite Sn isotope values. To test this, we compared the sample CZR ST 03 measured in two different locations (sample A at the University of Arizona and sample B at Rutgers reported in Table 1). The reported values represent two different powdered portions processed individually from the same stannite mineral separate. Notice that the values fall within the error range described above. Further discussion about the details of analysis and error calculation can be found in Mathur et al. (2017).

## RESULTS

The Sn isotope values for a total of 71 samples (50 cassiterite and 21 stannite samples) are reported in Figures 2 and 3, and Table 1. Natural mass-dependent fractionation is evident, as the slope of δ<sup>124</sup>Sn vs. δ<sup>120</sup>Sn is 2 with an r<sup>2</sup> = 0.99 (Fig. 2). The two minerals show statistically distinct populations regardless of deposit type, where cassiterite has a higher mean δ<sup>124</sup>Sn value [+0.48 ± 0.62‰ (1σ)] than stannite δ<sup>124</sup>Sn [−1.47 ± 0.54‰ (1σ)], i.e., a difference of about 2‰.

The reported data are in accord with previous studies. Hausteina et al. (2010) report 30 Sn isotope values for Cornish cassiterite. Only one analysis of stannite has been published, with Brüggmann et al. (2017) documenting the composition of a sample from Cornwall that was prepared for analysis by co-smelting with copper metal, rather than aqua regia dissolution. Both studies used an in-house standard (Puratronic high-purity foil) for which Brüggmann et al. (2017) provided a comparative

**TABLE 1.** Deposit location, mineral phase, and Sn isotope data for each sample

Study no.	Country	Region	Mineral	δ <sup>120</sup> Sn ‰	δ <sup>124</sup> Sn ‰
BOL 06	Bolivia	Oruro	Cassiterite	0.06	0.08
BOL 07	Bolivia	Potosi	Cassiterite	−0.32	−0.60
BOL 08	Bolivia	Potosi	Cassiterite	0.39	0.70
BOL 09	Bolivia	Potosi	Cassiterite	0.38	0.71
BOL 10	Bolivia	Potosi	Cassiterite	0.20	0.33
BOL 11	Bolivia	Potosi	Cassiterite	0.40	0.80
BOL 12	Bolivia	Potosi	Cassiterite	0.48	0.89
BOL 13	Bolivia	Potosi	Cassiterite	0.31	0.58
BOL 14	Bolivia	Potosi	Cassiterite	0.21	0.40
CZR 01	Czech Republic	Erzgebirge	Cassiterite	0.43	0.81
CZR 02	Czech Republic	Erzgebirge	Cassiterite	0.26	0.48
CZR 03	Czech Republic	Erzgebirge	Cassiterite	0.02	0.11
CZR 04	Czech Republic	Erzgebirge	Cassiterite	0.07	0.20
CZR 05	Czech Republic	Erzgebirge	Cassiterite	0.51	0.97
CZR 06	Czech Republic	Erzgebirge	Cassiterite	0.60	1.12
CZR 07	Czech Republic	Erzgebirge	Cassiterite	0.57	1.11
CZR 08	Czech Republic	Erzgebirge	Cassiterite	0.58	1.07
CZR 09	Czech Republic	Erzgebirge	Cassiterite	0.03	0.01
CZR 10	Czech Republic	Erzgebirge	Cassiterite	0.48	0.90
CZR 11	Czech Republic	Erzgebirge	Cassiterite	0.58	1.08
CZR 12	Czech Republic	Erzgebirge	Cassiterite	0.56	1.02
CZR 13	Czech Republic	Erzgebirge	Cassiterite	−0.02	−0.12
CZR 14	Czech Republic	Erzgebirge	Cassiterite	0.69	1.23
CZR 15	Czech Republic	Erzgebirge	Cassiterite	0.28	0.50
CZR 16	Czech Republic	Erzgebirge	Cassiterite	0.39	0.90
CZR 17	Czech Republic	Erzgebirge	Cassiterite	0.39	0.75
CZR 18	Czech Republic	Erzgebirge	Cassiterite	0.46	0.77
CZR 19	Czech Republic	Erzgebirge	Cassiterite	0.51	0.91
CZR 20	Czech Republic	Erzgebirge	Cassiterite	−0.17	−0.37
CZR 21	Czech Republic	Erzgebirge	Cassiterite	0.70	1.27
CZR 22	Czech Republic	Erzgebirge	Cassiterite	0.26	0.44
ENG 01	England	Cornwall	Cassiterite	0.52	1.09
ENG 02	England	Cornwall	Cassiterite	0.67	1.20
ENG 03	England	Cornwall	Cassiterite	0.39	0.75
ENG 04	England	Cornwall	Cassiterite	0.28	0.68
ENG 08	England	Cornwall	Cassiterite	0.57	1.13
ENG 09	England	Cornwall	Cassiterite	0.42	0.82
ENG 10	England	Cornwall	Cassiterite	0.25	0.54
ENG 11	England	Cornwall	Cassiterite	0.30	0.56
ENG 13	England	Cornwall	Cassiterite	0.43	0.80
ENG 14	England	Cornwall	Cassiterite	0.44	0.81
ENG 15	England	Cornwall	Cassiterite	0.47	0.87
USA 01	U.S.A.	South Dakota	Cassiterite	−0.60	−1.18
USA 02	U.S.A.	South Dakota	Cassiterite	0.04	0.12
USA 03	U.S.A.	South Dakota	Cassiterite	−0.61	−1.14
USA 04	U.S.A.	South Dakota	Cassiterite	−0.19	−0.32
USA 05	U.S.A.	South Dakota	Cassiterite	−0.02	−0.02
USA 06	U.S.A.	South Dakota	Cassiterite	−0.04	−0.09
USA 07	U.S.A.	South Dakota	Cassiterite	−0.57	−1.10
USA 08	U.S.A.	South Dakota	Cassiterite	−0.32	−0.57
CZR ST 03a	Czech Republic	Erzgebirge	Stannite	−0.65	−1.18
CZR ST 03b	Czech Republic	Erzgebirge	Stannite	−0.60	−1.25
BOL 15	Bolivia	Potosi	Stannite	−0.91	−1.84
BOL 16	Bolivia	Potosi	Stannite	0.00	−0.27
BOL 18	Bolivia	Oruro	Stannite	−0.86	−1.83
BOL 19	Bolivia	Oruro	Stannite	−0.55	−1.12
BOL 20	Bolivia	Oruro	Stannite	−0.59	−0.88
BOL 21	Bolivia	Potosi	Stannite	−0.51	−0.87
CZR 23	Czech Republic	Erzgebirge	Stannite	−0.98	−1.56
CZR 24	Czech Republic	Erzgebirge	Stannite	−0.51	−1.13
ENG 16	England	Cornwall	Stannite	−0.81	−1.46
ENG 17	England	Cornwall	Stannite	−0.62	−1.15
ENG 18	England	Cornwall	Stannite	−0.57	−1.38
ENG 19	England	Cornwall	Stannite	−0.89	−1.59
ENG 20	England	Cornwall	Stannite	−0.94	−1.87
ENG 21	England	Cornwall	Stannite	−0.81	−1.46
ENG 22	England	Cornwall	Stannite	−0.62	−1.15
ENG 23	England	Cornwall	Stannite	−0.57	−1.38
ENG 24	England	Cornwall	Stannite	−0.89	−1.59
ENG 25	England	Cornwall	Stannite	−0.94	−1.87
USA 09	U.S.A.	South Dakota	Stannite	−1.12	−2.41
USA 10	U.S.A.	South Dakota	Stannite	−1.71	−2.88

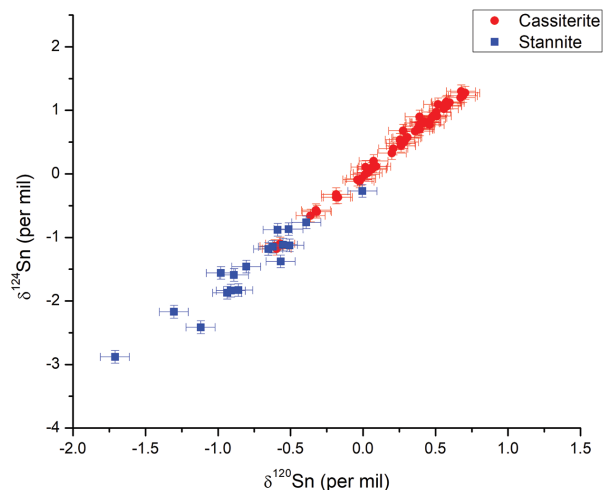


**FIGURE 2.** Mass dependence of cassiterite and stannite data, the slope of the presented line = 2. The relative clustering of the different minerals is evident. (Color online.)

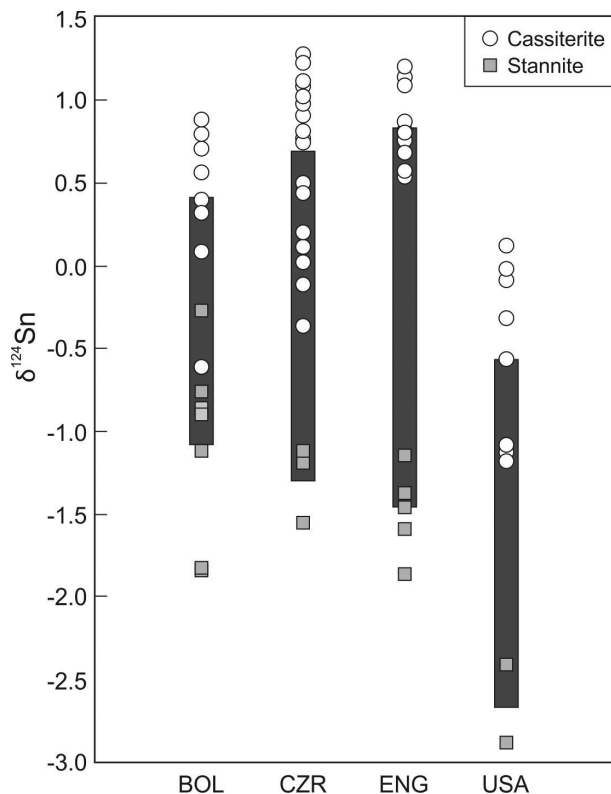


**FIGURE 3.** Tin isotope ranges of the minerals for each deposit. Gray bars indicate range of cassiterite and stannite values for each deposit.

value for NIST 3161a used herein, allowing for data conversion. The converted mean  $\delta\text{Sn}$  of  $0.11 \pm 0.08\text{‰}$  per amu for cassiterite from Cornwall reported by Hausteiner et al. (2010) is statistically equivalent to the findings of this study ( $0.12 \pm 0.03\text{‰}$  per amu;  $n = 11$ ). Furthermore, both Brüggemann et al. (2017) and this study found a distinctly lower value of  $\delta\text{Sn}$  for Cornish stannite rela-

tive to NIST 3161a,  $-0.06 \pm 0.05\text{‰}$  per amu ( $n = 1$ ) and  $-0.19 \pm 0.04\text{‰}$  per amu ( $n = 5$ ), respectively. This reproducibility demonstrates that differing preparation methods yield consistent analytical results for both cassiterite and stannite. No published data sets of Sn isotope compositions exist for minerals from Bolivia or South Dakota.

The mean values of cassiterite and stannite show similar variation across the four deposits studied, with a  $\delta^{124}\text{Sn}$  range of 2.48‰ for cassiterite and 2.61‰ for stannite. However, in each of the four deposits studied, Sn in stannite has lower values than cassiterite. To quantify this relationship, a comparison of the mean values of the two phases within different deposits was calculated using the following expression:

$$\Delta^{124}\text{Sn}_{\text{cassiterite-stannite}} = \text{mean } \delta^{124}\text{Sn}_{\text{cassiterite}} - \text{mean } \delta^{124}\text{Sn}_{\text{stannite}}$$

Tin mineralization from all four ore districts has similar values:  $2.3 \pm 0.2\text{‰}$  (Cornwall),  $2.1 \pm 0.2\text{‰}$  (South Dakota),  $2.0 \pm 0.2\text{‰}$  (Cinovec-Krupka), and  $1.5 \pm 0.2\text{‰}$  (Bolivia) (Fig. 2). Thus, each locality displays a similar and consistent shift in Sn isotopic composition between cassiterite and stannite regardless of mineralization style and depth of emplacement. However, the shallowest deposits are associated with the lowest  $\Delta^{124}\text{Sn}_{\text{cassiterite-stannite}}$  values.

### INSIGHTS INTO CAUSES OF SN ISOTOPE FRACTIONATION IN ORES

Fractionation of Sn isotopes in hydrothermal mineralizing systems may be related to multiple inter-related variables: speciation of Sn into different compounds in solution, liquid-vapor partitioning, electron transfer, temperature, pressure, the competitive bonding environment, and equilibrium processes associated with partitioning of Sn into different phases. There is a dearth of experimental studies that isolate these factors associated with ore deposit genesis. However, empirical evidence derived from ore minerals associated with known geochemical reactions and processes have been used commonly as a means to constrain the causes for isotopic fractionation in mineralizing systems using other metal isotope systems: Fe (Bilenker et al. 2016; Zhu et al. 2018), Ni (Liu et al. 2018), Cu (Markl et al. 2006; Maher et al. 2011, 2013), Zn (Gagnevin et al. 2012; Zhou et al. 2014), Mo (Greber et al. 2011; Yao et al. 2016), Ag (Mathur et al. 2018), and Te (Fornadel et al. 2014).

Given the geological context of the samples, several of the above mechanisms can be eliminated. The consistent variation of Sn isotope values between cassiterite and stannite presented here persists for deposits that formed in deep vapor-absent environments (pegmatites of South Dakota) up to the subvolcanic settings (porphyries in Bolivia), indicating that pressure changes, temperature variations, and liquid-vapor transitions cannot be the causative mechanism for the observed fractionation. The similarities in mineralogical paragenesis in these systems (where cassiterite in these systems clearly predates stannite and no co-genetic sulfides exist with cassiterite) excludes equilibrium partitioning among phases or within-solution speciation as a clear-cut mechanism. As demonstrated by Eugster (1985), Sn in hydrothermal tin systems is in the form of chloride complexes.  $\text{SnO}_2$  has a broad stability field at high  $T$ , while with decreasing temperature the stannite field expands.

Differing bond energies associated with precipitation of Sn with O and S could be related to fractionation. The bond distance difference between the two ligands is 0.25 pm (Smith 2012). Theoretical fractionation factors can be calculated using these bond lengths (as has been done with other metal isotopes, Seo et al. 2007), however as pointed out with Fe isotope fractionation factors determined by (Sossi and O'Neill 2017) a significant discrepancy exists between theoretical and experimental determined fractionation factors. Nevertheless, the potential exists that within solution speciation may affect fractionation when Sn-O and Sn-Cl species exist during precipitation of cassiterite. Germane to this argument, given the mass balance that must occur in the system and that no sulfides form paragenetically early in these systems, the initial redox of Sn from the hydrothermal solution is the most likely mechanism for fractionation.

It is well established that tin is transported in hydrothermal fluids in the reduced state ( $\text{Sn}^{2+}$ ), and that formation of cassiterite and stannite requires an oxidative transition to  $\text{Sn}^{4+}$ . Furthermore, it has been demonstrated repeatedly that oxidation of multi-valent metals imparts significant isotopic fractionation favoring the heavy isotope (Domagal-Goldman and Kubicki 2008; Dauphas et al. 2009, 2014; Sherman 2013). For some metals, such as Cu, oxidation-induced fractionation is observed in the products of low-temperature, near-surface reactions (Mathur et al. 2010). In cases such as Fe, identifying the component of fractionation associated with redox reactions is confounded by overprints due to numerous coincident fractionation mechanisms, particularly partitioning between coexisting phases (Dauphas et al. 2014). Neither weathering, nor partitioning between coexisting phases, complicate the Sn system in the hydrothermal setting examined in this study.

Based on inelastic nuclear resonant X-ray scattering (INRXS) and Mössbauer spectroscopy experiments, Polyakov et al. (2005) predicted that oxidation state would have a large effect on fractionation of Sn. Since neither low-temperature processes nor partitioning between co-precipitating minerals complicate the hydrothermal Sn isotopic system examined here, fractionation due to high-temperature redox changes likely would be evident. In each of the four tin camps studied there is a large Sn isotopic variation between early cassiterite and later stannite, between 1.5 and 2.4‰ in  $\delta^{124}\text{Sn}$ . Given the oxidation-dependent mechanism for cassiterite precipitation (Heinrich 1990), and the results of the synchrotron experiments of Polyakov et al. (2005), this isotopic shift is most likely attributable to the oxidation of  $\text{Sn}^{2+}$  in the hydrothermal fluids. Oxidation-driven precipitation of cassiterite left the hydrothermal solution enriched in tin of lighter isotopic composition. Subsequent oxidation of the residual  $\text{Sn}^{2+}$  resulted in the precipitation of stannite with negative  $\delta^{124}\text{Sn}$  values, inheriting the residual Sn isotope composition of the fluid. It is also possible that within solution speciation of Sn-S and Sn-O bonds could impart some degree of fractionation.

The fractionation factor and relative mass of Sn residing in different reservoirs can be approximated and used to model Sn isotope values in cassiterite and stannite. Creech et al. (2017) provide an Sn isotopic composition of the USGS standard GSP-2 ( $\delta^{122}\text{Sn} = +0.19\text{‰}$ , where  $\delta^{122}\text{Sn}$  is  $^{122}\text{Sn}/^{118}\text{Sn}$  and is equivalent to  $\delta^{120}\text{Sn}$  presented here), a granodiorite from the ca. 1400 Ma metaluminous to peraluminous Silver Plume granitoid suite, Colorado (Bender

1983). This is the only granitic Sn isotope composition reported in the literature. Although the standards used to bracket the data in Creech et al. (2017) and here are different, Brüggemann et al. (2017) point out that several ICP-MS standards are within 0.1‰ of the 3160 NIST standard reported here, and thus adequate to construct a first-order geochemical model. A Proterozoic lower crust is the likely source for the generation of the Erzgebirge tin-granites (Bankwitz and Bankwitz 1994). Accordingly, GSP-2 is adopted as a reasonable starting composition for the tin composition of magmas ( $\delta^{124}\text{Sn} = +0.40\text{‰}$ ) associated with the Erzgebirge, which corresponds to a fractionation factor between the starting fluid and average cassiterite of  $\alpha_{\text{solution-solid}} = 1.0003$ . Rayleigh distillation equations presented in Faure (1986) yield results where the first 80% (Fig. 4) of the Sn precipitated from the hydrothermal fluid would have  $\delta^{124}\text{Sn}$  values between 0.2 to +0.6‰, which is congruent with the distribution of Sn isotope values for Cornwall, Erzgebirge, and Bolivia in Table 1.

The model also demonstrates that to obtain solutions and solids corresponding to the stannite values, greater than 99.5% all of Sn in the system must have precipitated in the form of cassiterite. This is consistent with the relative abundance of these two minerals in tin ores globally; although stannite is widely distributed in sulfide ores associated with tin mineralization, it is a very minor component and rarely of economic interest. Even if the fractionation factor is doubled, the model still predicts the Sn isotope values documented in cassiterite and stannite. The mass balance of the solutions in this model dictates that the remaining solutions must possess a significantly larger proportion of lighter Sn when the stannite is formed in the system.

While it is possible that Sn-S bonding from solution to solid would induce the fractionation seen, the mass balance of Sn in the system predicts that the remaining solution must possess proportionately significant lighter Sn. Therefore, the simple distillation

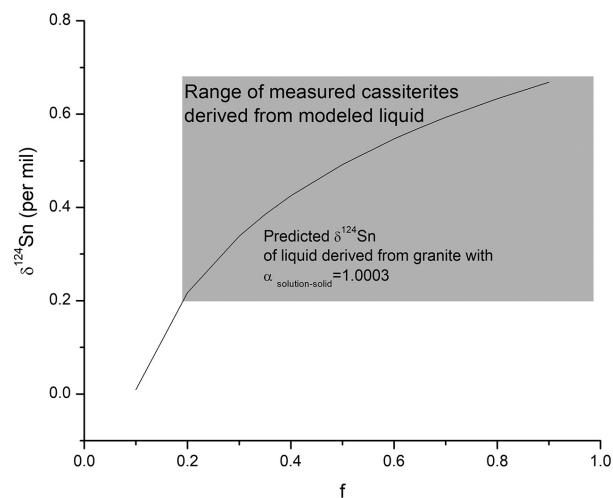


**FIGURE 4.** Rayleigh distillation model that predicts the range of fluids that would evolve from a granitic magma where  $f$  is a proportion of Sn in magma/Sn in fluid. The gray box highlights the range of Sn isotope values for cassiterite assuming fractionation occurred during redox reactions that led to the precipitation of cassiterites. The model predicts cassiterite with the largest Sn isotope value precipitated earliest.

model predicts the range of Sn isotope values observed in both phases using a fractionation factor most likely triggered by electron transfer in the hydrothermal solution. Further higher temperature experimentation will elucidate if redox is the sole mechanism or different bonding energies associated with the formation of Sn-S to form stannite control fractionation.

Although oxidation-related isotopic fractionation is evident in the four localities regardless of mineralization style, there is a range of the  $\Delta^{124}\text{Sn}_{\text{cassiterite-stannite}}$  values. This variation could be due to variations in the efficiency of cassiterite precipitation; lower yields of early cassiterite would result in lower values of  $\Delta^{124}\text{Sn}_{\text{cassiterite-stannite}}$ . Alternatively, this range could be related to additional fractionation mechanisms. Partitioning of Sn between brine and vapor in a shallow setting likely induces fractionation, similar to that observed in the distillation experiments of Mathur et al. (2017). Fractionation due to the partitioning of Sn between vapor and fluid at shallow depths could impart a shift in the isotopic composition of the fluids from which stannite precipitates. This would be consistent with the observed variation in  $\Delta^{124}\text{Sn}_{\text{cassiterite-stannite}}$  values and standard deviation of  $\delta^{124}\text{Sn}$  of cassiterite from the hydrothermal ores: highest  $\Delta^{124}\text{Sn}_{\text{cassiterite-stannite}}$  (2.3) and lowest standard deviation ( $\pm 0.21\%$ ) at Cornwall with the greatest emplacement depth (5–6 km; Pownall et al. 2012; Drivenes et al. 2016), lower ( $2.0 \pm 0.46$ ) at Cinovec (Zinnwald) at intermediate depth (1–2 km; Korges et al. 2018), and lowest  $\delta^{124}\text{Sn}_{\text{cassiterite-stannite}}$  (1.5) for the shallowest deposits in Bolivia (<1.5 km; Sillitoe et al. 1975) (Fig. 3).

#### IMPLICATIONS AND FUTURE DIRECTIONS FOR SN ISOTOPIC ANALYSIS

The current study demonstrates that oxidation of Sn at high temperature causes predictable fractionation of Sn isotopes. Fractionation of the Sn isotope system may provide a better monitor of high-temperature redox reactions than those in which such signatures may be masked by isotopic partitioning between coexisting phases (e.g., Fe). Furthermore, the stability of cassiterite in the surface environment preserves its isotopic signature throughout the weathering process. Accordingly, Sn isotopes have great potential as a broadly applicable analytical tool. They may be used to identify source rocks and monitor redox changes in magmatic-hydrothermal systems, even in highly weathered settings. Sn isotopic analysis can also provide insights into the processes associated with rare-element granite mineralization. In addition, Sn isotope analysis is a powerful tool for provenance studies of bronze artifacts, allowing archaeologists to match artifacts to a known tin source or to refine their search parameters for a specific tin source by inferring deposit characteristics from the Sn isotope signatures of bronze artifacts.

#### ACKNOWLEDGMENTS

This work is supported by the National Key R&D Program of China (2016YFC0600405), the GIGCAS No.IS-2547, the National Natural Science Foundation of China (nos. 41672079 and 41372085), and Strategic Priority Research Program (B) of the Chinese Academy of Sciences (XDB1803206).

#### REFERENCES CITED

- Badullovich, N., Moynier, F., Creech, J., Teng, F., and Sossi, P. (2017) Tin isotopic fractionation during igneous differentiation and Earth's mantle deposition. *Geochemical Perspectives Letters*, 5, 24–28.
- Balliana, E., Aramendia, M., Resano, M., Barbante, C., and Vanhaecke, F. (2013) Copper and tin isotopic analysis of ancient bronzes for archaeological investigation: development and validation of a suitable analytical methodology. *Analytical and Bioanalytical Chemistry*, 405, 2973–2986.
- Bankwitz, P., and Bankwitz, E. (1994) Crustal structure of the Erzgebirge: Metallogeny of Collisional Orogens. Czech Geological Survey, Prague, 20–34.
- Bender, R.B. (1983) Petrology and geochemistry of the Silver Plume-age plutons of the southern and central Wet Mountains, Colorado. Unpublished Ph.D. thesis, Louisiana State University, Baton Rouge, 200p.
- Bilenker, L.D., Simon, A.C., Reich, M., Lundstrom, C.C., Gajos, N., Bindeman, I., Barra, F., and Munizaga, R. (2016) Fe–O stable isotope pairs elucidate a high-temperature origin of Chilean iron oxide-apatite deposits: *Geochimica et Cosmochimica Acta*, 177, 94–104.
- Borrok, D., Nimick, D., Wanty, R., and Ridley, W. (2008) Isotopic variations of dissolved copper and zinc in stream waters affected by historical mining. *Geochimica et Cosmochimica Acta*, 72, 329–344.
- Bromley, A., and Holl, C. (1986) Tin mineralization in Southwest England. In B. Wills and R. Barley, Eds., *Mineral Processing at a Crossroads*, p. 195–262. *Matrinus Nijhoff*.
- Brügmann, G., Berger, D., and Pernicka, E. (2017) Determination of the tin stable isotopic composition in tin-bearing metals and minerals by MC-ICP-MS. *Geostandards and Geoanalytical Research*, 41, 437–448.
- Campbell, A., and Panter, K. (1990) Comparison of fluid inclusions in coexisting (cogenetic?) wolframite, cassiterite, and quartz from St. Michael's Mount and Cligga Head, Cornwall, England. *Geochimica et Cosmochimica Acta*, 54, 673–681.
- Černý, P., Masau, M., Ericit, T.S., Chapman, R., and Chackowsky, L. (2001) Stannite and kesterite from the Peerless pegmatite, Black Hills, South Dakota, USA. *Journal of the Czech Geological Society*, 46, 27–33.
- Černý, P., Blevin, P., Cuney, M., and London, D. (2005) Granite-related ore deposits. In J. Heldenquist, J. Thompson, R. Goldfarb, and J. Richards, Eds., *Economic Geology One Hundredth Anniversary Volume 1905–2005*, p. 337–370. *Society of Economic Geologists*.
- Chen, X.C., Hu, R.Z., Bi, X.W., Li, H.M., Lan, J.B., Zhao, C.H., and Zhu, J.J. (2014) Cassiterite LA-MC-ICP-MS U/Pb and muscovite  $^{40}\text{Ar}/^{39}\text{Ar}$  dating of tin deposits in the Tengchong-Lianghe tin district, NW Yunnan, China. *Mineralium Deposita*, 49, 843–860.
- Chicharro, E., Boiron, M.C., Lopez-Garcia, J., Barfod, D., and Villaseca, C. (2016) Origin, ore forming fluid evolution and timing of the Logrosán Sn-(W) ore deposits (Central Iberian Zone, Spain). *Ore Geology Reviews*, 72, 896–913.
- Connolly, J. (1916) Rare minerals in the Black Hills as state assets. *Proceedings of the South Dakota Academy of Science*, 1, 40–53.
- Creech, J.B., Moynier, F., and Badullovich, N. (2017) Tin stable isotope analysis of geological materials by double-spike MC-ICPMS. *Chemical Geology*, 457, 61–67.
- Dauphas, N., Craddock, P.R., Asimow, P.D., Bennett, V.C., Nutman, A.P., and Ohnenstetter, D. (2009) Iron isotopes may reveal the redox conditions of mantle melting from Archean to Present. *Earth and Planetary Science Letters*, 288, 255–267.
- Dauphas, N., Roskosz, M., Alp, E., Neuville, D., Hu, M., Sio, C., Tissot, F., Zhao, J., Tissandier, L., and Médard, E. (2014) Magma redox and structural controls on iron isotope variations in Earth's mantle and crust. *Earth and Planetary Science Letters*, 398, 127–140.
- Domagal-Goldman, S.D., and Kubicki, J.D. (2008) Density functional theory predictions of equilibrium isotope fractionation of iron due to redox changes and organic complexation. *Geochimica et Cosmochimica Acta*, 72, 5201–5216.
- Drivenes, K., Larsen, R., Müller, A., and Sørensen, B. (2016) Crystallization and uplift path of late Variscan granites evidenced by quartz chemistry and fluid inclusions: Example from the Land's End granite, SW England. *Lithos*, 252–253, 57–75.
- Eibschütz, M., Hermon, E., and Shtrikman, S. (1967) Determination of cation valencies in  $\text{Cu}_2\text{Fe}^{119}\text{SnS}_4$  by Mössbauer effect and magnetic susceptibility measurements. *Journal of Physics and Chemistry of Solids*, 28, 1633–1636.
- Eugster, H., and Wilson, G. (1985) Transport and deposition of ore-forming elements in hydrothermal systems associated with granites. In C. Halls, Ed., *High heat production (HPP) granites, hydrothermal circulation and ore genesis*, p. 87–98. *Institution of Mining and Metallurgy*.
- Farges, F., Linnen, R., and Brown, G. Jr. (2006) Redox and speciation of tin in hydrous silicate glasses: A comparison with Nb, Ta, Mo and W. *Canadian Mineralogist*, 44, 795–810.
- Faure, G. (1986) *Principles of Isotope Geology*. Wiley.
- Fornadel, A.P., Spry, P.G., Jackson, S.E., Mathur, R.D., Chapman, J.B., and Girard, I. (2014) Methods for the determination of stable Te isotopes of minerals in the system Au-Ag-Te by MC-ICP-MS. *Journal of Analytical Atomic Spectrometry*, 29, 623–637.
- Gagnevin, D., Boyce, A.J., Barrie, C.D., Menuge, J.F., and Blakeman, R.J. (2012) Zn, Fe and S isotope fractionation in a large hydrothermal system. *Geochimica et Cosmochimica Acta*, 88, 183–198.
- Greber, N.D., Hofmann, B.A., Voegelin, A.R., Villa, I.M., and Nägler, T.F. (2011) Mo isotope composition in Mo-rich high- and low-*T* hydrothermal systems from the Swiss Alps. *Geochimica et Cosmochimica Acta*, 75, 6600–6609.
- Greenwood, N., and Whitfield, H. (1968) Mössbauer effect studies on cubanite ( $\text{CuFe}_2\text{S}_3$ ) and related iron sulphides. *Journal of the Chemical Society A: Inorganic Physical Theoretical*, 7, 1697–1699.
- Groves, D.I. (1972) The geochemical evolution of tin-bearing granites in the Blue Tier

- batholith, Tasmania. *Economic Geology*, 67, 445–457.
- Haustein, M., Gillis, C., and Pernicka, E. (2010) Tin isotopy—a new method for solving old questions. *Archaeometry*, 52, 816–832.
- Heinrich, C. (1990) The chemistry of hydrothermal tin(tungsten) ore deposition. *Economic Geology*, 85, 457–481.
- Heinrich, C., and Ryan, C. (1992) Mineral paragenesis and regional zonation of granite-related Sn-As-Cu-Pb-Zn deposits: A chemical model for the Mole Granite district (Australia) based on PIXE fluid inclusion analyses. In Y. Kharaka and A. Maest, Eds., *Water-Rock Interaction*, p. 1583–1587. Proceedings on the 7th International Symposium on Water-Rock Interaction.
- Imeokparia, E. (1982) Tin content of biotites from the Afu younger granite complex, Central Nigeria. *Economic Geology*, 77, 1710–1724.
- Jackson, N., Halliday, A., Sheppard, S., and Mitchell, J. (1982) Hydrothermal activity in the St. Just mining district, Cornwall, England. In A. Evans, Ed., *Metalization Associated with Acid Magmatism*, p. 137–179. Wiley.
- Jackson, N., Willis-Richards, J., Manning, D., and Sams, M. (1989) Evolution of the Cornubian Ore Field, Southwest England: Part II. Mineral deposits and ore-forming processes. *Economic Geology*, 84, 1101–1133.
- Kelly, W., and Turneure, F. (1970) Mineralogy, paragenesis and geothermometry of the tin and tungsten deposits of the Eastern Andes, Bolivia. *Economic Geology*, 65, 609–680.
- Korges, M., Weis, P., Lüders, V., and Laurent, O. (2018) Depressurization and boiling of a single magmatic fluid as a mechanism for tin-tungsten deposit formation. *Geology*, 46, 75–78.
- Lehmann, B. (1982) Metallogeny of tin: Magmatic differentiation versus geochemical heritage. *Economic Geology*, 77, 50–59.
- (1987) Tin granites, geochemical heritage, magmatic differentiation. *Geologische Rundschau*, 76, 177–185.
- (1990) *Metallogeny of Tin*. Springer, 211 p.
- Limmen, R., Pichavant, M., Holtz, F., and Burgess, S. (1995) The effect of  $f_{O_2}$  on the solubility, diffusion, and speciation of tin in haplogranitic melt at 850°C and 2 kbar. *Geochimica et Cosmochimica Acta*, 59, 1579–1588.
- Limmen, R., Pichavant, M., and Holtz, F. (1996) The combined effects of  $f_{O_2}$  and melt composition on SnO<sub>2</sub> solubility and tin diffusivity in haplogranitic melts. *Geochimica et Cosmochimica Acta*, 60, 4965–4976.
- Liu, S., Li, Y., Ju, Y., Liu, J., Liu, J., and Shi, Y. (2018) Equilibrium nickel isotope fractionation in nickel sulfide minerals. *Geochimica et Cosmochimica Acta*, 222, 1–16.
- London, D. (1984) Experimental phase equilibria in the system LiAlSiO<sub>3</sub>-SiO<sub>2</sub>-H<sub>2</sub>O: a petrogenetic grid for lithium-rich pegmatites. *American Mineralogist*, 69, 995–1004.
- Maher, K.C., Jackson, S., and Mountain, B. (2011) Experimental evaluation of the fluid–mineral fractionation of Cu isotopes at 250°C and 300°C. *Chemical Geology*, 286, 229–239.
- Markl, G., and Schumacher, J. (1996) Spatial variations in temperature and composition of greisen-forming fluids: An example from the Variscan Triberg Granite Complex, Germany. *Economic Geology*, 91, 576–589.
- Markl, G., Lahaye, Y., and Schwinn, G. (2006) Copper isotopes as monitors of redox processes in hydrothermal mineralization. *Geochimica et Cosmochimica Acta*, 70, 4215–4228.
- Mason, A., Powell, W., Bankoff, H., Mathur, R., Bulatović, A., Filipović, V., and Ruiz, J. (2016) Tin isotope characterization of bronze artifacts of the central Balkans. *Journal of Archaeological Science*, 69, 110–117.
- Mathur, R., Dendas, M., Titley, S., and Phillips, A. (2010) Patterns in the copper isotopic composition of minerals in porphyry copper deposits in the Southwestern United States of America. *Economic Geology*, 105, 1457–1467.
- Mathur, R., Munk, L., Nguyen, M., Gregory, M., Ansell, H., and Lang, J. (2013) Modern and paleofluid pathways revealed by Cu isotope compositions in surface waters and ores of the Pebble porphyry Cu-Au-Mo deposit, Alaska. *Economic Geology*, 108, 529–541.
- Mathur, R., Powell, W., Mason, A., Godfrey, L., Yao, J., and Baker, M.E. (2017) Preparation and measurement of cassiterite for Sn isotope analysis. *Geostandards and Geoanalytical Research*, 41, 701–707.
- Mathur, R., Arribas, A., Megaw, P., Wilson, M., Stroup, S., Meyer-Arrivillaga, D., and Arribas, I. (2018) Fractionation of silver isotopes in native silver explained by redox reactions. *Geochimica et Cosmochimica Acta*, 224, 313–326.
- Neiva, A. (1976) The geochemistry of biotites from granites of northern Portugal with special reference to their tin content. *Mineralogical Magazine*, 40, 453–466.
- Plimer, I. (1984) Malayaite and tin-bearing silicates from a skarn at Doradilla via Bourke, New South Wales. *Australian Journal of Earth Sciences*, 31, 147–153.
- (1987) Fundamental parameters for the formation of granite-related tin deposits. *Geologische Rundschau*, 76, 23–40.
- Pokrovsky, O., Viers, J., Emnova, E., Kompantseva, E., and Freydier, R. (2008) Copper isotope fractionation during its interaction with soil and aquatic microorganisms and metal oxy(hydr)oxides; possible structural control. *Geochimica et Cosmochimica Acta*, 72, 1742–1757.
- Polyakov, V., Mineev, S., Clayton, R., Hu, G., and Mineev, K. (2005) Determination of equilibrium isotope fractionation factors from synchrotron radiation experiments. *Geochimica et Cosmochimica Acta*, 69, 5531–5536.
- Pownall, J., Waters, D., Searle, M., Shail, R., and Robb, L. (2012) Shallow laccolithic emplacement of the Land's End and Tregonning granites, Cornwall, U.K.: Evidence from aureole field relations and *P-T* modeling of cordierite-anthophyllite hornfels. *Geosphere*, 8, 1467–1504.
- Radivojević, M., Rehren, T., Kuzmanović-Cvetković, J., Jovanović, M., and Northover, J. (2013) Tainted ores and the rise of tin bronze metallurgy, c. 6500 years ago. *Antiquity*, 87, 1030–1045.
- Rudnick, R., and Gao, S. (2003) Composition of the continental crust. *Treatise on Geochemistry*, 3, 1–64.
- Schwartz, G. (1925) *Geology of the Etta spodumene mine, Black Hills, South Dakota*. *Economic Geology*, 20, 646–659.
- Seo, J.H., Lee, S.K., and Lee, I. (2007) Quantum chemical calculations of equilibrium copper (I) isotope fractionations in ore-forming fluids. *Chemical Geology*, 243, 225–237.
- Sherman, D.M. (2013) Equilibrium isotopic fractionation of copper during oxidation/reduction, aqueous complexation and ore-forming processes: Predictions from hybrid density functional theory. *Geochimica et Cosmochimica Acta*, 118, 85–97.
- Sillitoe, R., Halls, C., and Grant, J. (1975) Porphyry tin deposits in Bolivia. *Economic Geology*, 70, 913–927.
- Smith, P.J. (2012) *Chemistry of Tin*. Springer, 578 p.
- Smith, M., Banks, D., Yardley, B., and Boyce, A. (1996) Fluid inclusion and stable isotope constraints on the genesis of the Cligga Head Sn-W deposit, S. W. England. *European Journal of Mineralogy*, 8, 961–974.
- Sossi, P.A., and O'Neill, H.St.C. (2017) The effect of bonding environment on iron isotope fractionation between minerals at high temperature. *Geochimica et Cosmochimica Acta*, 196, 121–143.
- Sugaki, A., and Kitakaze, A. (1988) Tin-bearing minerals from Bolivian polymetallic deposits and their mineralization stages. *Mining Geology*, 38, 419–435.
- Sugaki, A., Ueno, H., Shimada, M., Kitakaze, A., Shima, H., Sansines, O., and Saavedra, A. (1981) Geological study on polymetallic hydrothermal deposits in the Oruro District, Bolivia. *Science Reports, Tohoku University, Series 3: Mineralogy, Petrology, and Economic Geology*, 15, 1–52.
- Taylor, R. (1979) The geology of tin deposits. In *Developments in Economic Geology*, vol. 11, 543 p. Elsevier.
- Wang, R., Xie, L., Chen, J., Yu, A., Wang, L., Lu, J., and Zhu, J. (2013) Tin-carrier minerals in metaluminous granites of the western Nanling Range (southern China): Constraints on processes of tin mineralization in oxidized granites. *Journal of Asian Earth Sciences*, 74, 361–372.
- Xie, L., Wang, R.-C., Chen, J., and Zhu, J.-C. (2010) Mineralogical evidence for magmatic and hydrothermal processes in the Qitianling oxidized tin-bearing granite (Hunan, South China): EMP and (MC)-LA-ICPMS investigations of three types of titanite. *Chemical Geology*, 276, 53–68.
- Yamazaki, E., Nakai, S., Sahoo, Y., Yokoyama, T., Mifune, H., Saito, T., Chen, J., Takagi, N., Hokanishi, N., and Yasuda, A. (2014) Feasibility studies of Sn isotope composition for provenancing ancient bronzes. *Journal of Archaeological Science*, 52, 458–467.
- Yao, J., Mathur, R., Sun, W., Song, W., Chen, H., Mutti, L., Xiang, X., and Luo, X. (2016) Fractionation of Cu and Mo isotopes caused by vapor-liquid partitioning, evidence from the Dahutang W-Cu-Mo ore field. *Geochemistry, Geophysics, Geosystems*, 17, 1725–1739.
- Yuan, S., Peng, J., Hao, S., Li, H., Geng, J., and Zhang, D. (2011) In situ LA-MC-ICP-MS and ID-TIMS U–Pb geochronology of cassiterite in the giant Furong tin deposit, Hunan Province, South China: New constraints on the timing of tin–polymetallic mineralization. *Ore Geology Reviews*, 43, 235–242.
- Zhang, R., Lu, J., Wang, R., Yang, P., Zhu, J., Yao, Y., Gao, J., Li, C., Lei, Z., Zhang, W., and Guo, W. (2015) Constraints of in situ zircon and cassiterite U–Pb, molybdenite Re–Os and muscovite <sup>40</sup>Ar–<sup>39</sup>Ar ages on multiple generations of granitic magmatism and related W–Sn mineralization in the Wangxianling area, Nanling Range, South China. *Ore Geology Reviews*, 65, 1023–1042.
- Zhang, R., Lehmann, B., Seltmann, R., Sun, W., Li, C. (2017) Cassiterite U–Pb geochronology constrains magmatic-hydrothermal evolution in complex evolved granite systems: The classic Erzgebirge tin province (Saxony and Bohemia). *Geology*, 45, 1095–1098.
- Zhou, J.-X., Huang, Z.-L., Zhou, M.-F., Zhu, X.-K., and Muchez, P. (2014) Zinc, sulfur and lead isotopic variations in carbonate-hosted Pb–Zn sulfide deposits, southwest China. *Ore Geology Reviews*, 58, 41–54.
- Zhu, Z.-Y., Jiang, S.-Y., Mathur, R., Cook, N. J., Yang, T., Wang, M., Ma, L., and Ciobanu, C.L. (2018) Iron isotope behavior during fluid/rock interaction in K-feldspar alteration zone—A model for pyrite in gold deposits from the Jiadong Peninsula, East China. *Geochimica et Cosmochimica Acta*, 222, Supplement C, 94–116.

MANUSCRIPT RECEIVED FEBRUARY 24, 2018

MANUSCRIPT ACCEPTED JUNE 1, 2018

MANUSCRIPT HANDLED BY FANG-ZHEN TENG